Semiconductor Physics, Quantum Electronics & Optoelectronics, 2006. V. 9, N 2. P. 80-86.

PACS 72.80.Ey, 78.30.Fs

Synthesis and properties of semiconductor solid solutions $(InSb)_{1-x}(CdTe)_x$

E.F. Venger[1], L.M. Knorozok[2], L.Yu. Melnichuk[2], O.V. Melnichuk[2]
[1]*V. Lashkaryov Institute of Semiconductor Physics, NAS of Ukraine,*
41, prospect Nauky, 03028 Kyiv, Ukraine
[2]*Mykola Gogol Nizhyn State University, 2, Kropyv'yanskogo str., 16600 Nizhyn, Ukraine*

Abstract. We consider the growth technology and investigations of indium antimonide doped concurrently with acceptor (Cd) and donor (Te) impurities taken in equiatomic ratio. The optimal modes of single crystal synthesis and crystallization are determined. It is shown that, when doping the indium antimonide, its lattice parameter changes considerably. This leads to deformation of the electron energy spectrum, changes the bandgap and charge carrier effective mass and affects the optical and electrical properties of indium antimonide samples. As a result, such material becomes suitable for fabrication of IR photodetectors.

Keywords: indium antimonide, lattice parameter, effective mass, electron energy spectrum.

Manuscript received 04.03.06; accepted for publication 29.03.06.

1. Introduction

Further progress of advanced semiconductor electronics requires development of novel materials with preset properties and parameters, as well as both theoretical and experimental investigations of them. At present, a special emphasis is put upon studies of disordered systems. To simulate them, it is convenient to use heavily doped crystalline semiconductor binary compounds (e.g., $A^{III}B^{V}$), among which solid solutions (SS) hold a significant place. By studying them, it is possible to follow modification of the physical properties of the above compounds due to imperfections of the crystal lattice occurring at gradual replacement of anions or cations in it. Such studies also enhance substantially the possibilities to develop semiconductor devices on the basis of the abovementioned materials.

When the atomic (ionic) radii of dopants and host material are different, then a considerable local strain appears around the sites where an atom is replaced by another one. At high dopant concentration, this may lead to a considerable change of the lattice parameter of doped material, and this effect, in its turn, will result in modification of the electron energy spectrum. It was shown in [1] that in this case relative changes of the bandgap and effective mass of charge carriers may be order of magnitude bigger than relative change of material volume caused by strains. Such big relative changes of the bandgap and effective mass of charge carriers are particular characteristics of narrow-band semiconductors. A typical representative of such materials is indium antimonide doped concurrently with acceptor (Cd) and donor (Te) impurities taken in the equiatomic ratio. In this case, the atomic and ionic radii of the dopants differ essentially from those of the replaced atoms of the host material (indium antimonide).

In our previous works [2, 3], it was shown that, along with applied aspects, an important role in investigation of narrow-gap semiconductors with moderate and high degree of doping with specially chosen impurities belongs to theoretical and experimental studies how the properties of the host material depend on crystal lattice deformation, electron-deformation interaction and interaction between impurities, complexes formed by impurity atoms and those of host material, structural defects, *etc*.

The objective of this work is development of technology of synthesis of SS $(InSb)_{1-x}(CdTe)_x$, obtaining an information concerning the effect of its composition on the band structure parameters, and investigation of its optical and electrical properties in the course of concurrent doping the SS with the corresponding impurities.

2. Growth procedure and investigation of SS $(InSb)_{1-x}(CdTe)_x$

Synthesis of SS $(InSb)_{1-x}(CdTe)_x$ was carried out in a closed quartz container, at a controlled pressure of volatile component vapors. The starting materials were In, Sb, Cd and Te, with uncontrolled impurities of no more than

10^{-4} wt. %. The reagents were weighed with an analytical balance (within the error limits 5×10^{-4} g). Additional amounts of the volatile components (Sb and Cd) that were required to ensure an equilibrium pressure of their vapors in the crystallization zone were calculated according to the theory of ideal gases [4]. The container was pre-evacuated down to a pressure of 10^{-1}…10^{-3} Pa.

Before loading with substances, the ampoules were annealed at the temperatures 970…1020 °C for 8 to 10 h. After this, they were etched in a mixture of nitric and hydrofluoric acids for 20 to 40 min, and then several (3…5) times were washed off with distilled water.

The dopants were introduced immediately into the starting weight of substances. It was determined in the course of technological experiments that the reaction between the SS starting components proceeds up to an end. The distribution of impurities is more uniform when synthesis occurs at the temperatures 800…830 °C, *i.e.*, much over the InSb melting point (525 °C). Depending on the impurity concentration, time of synthesis was from 20 up to 100 h. To promote the process and ensure uniform distribution of impurities, a vibratory agitation of the melt was used sometimes.

We tested the horizontally- and vertically-oriented crystallization techniques to obtain $(InSb)_{1-x}(CdTe)_x$ crystals from melt. Based on our experimental studies of SS $(InSb)_{1-x}(CdTe)_x$, we gave preference to the horizontally-oriented crystallization. The following two versions of this technique were realized.

(i) Motion of the melt crystallization front was made automatically by decreasing the temperature in the furnace using a specially designed programmable facility. The starting temperature in the reactor was set within the range from 800 to 900 °C. After the synthesis process came to an end, the temperature was reduced manually (with the rate 70 to 100 °C/h) down to 540 °C, and then automatically (with the rate 3…5 °C/h) until the complete melt crystallization. When the temperature reached 470…480 °C, its further decrease was much faster (40 to 50 °C/h). Our technological experiments showed that this version is more appropriate for SS with rather low CdTe content (up to 0.5…1.0 mol. % CdTe in InSb).

(ii) According to another version, motion of the melt crystallization front was made by motion of the furnace with a preset velocity (0.5…3.0 mm/h) relatively to the stationary container with the melt. An abrupt temperature gradient in the crystallization zone was made using an additional spiral heater.

Fig. 1 shows the scheme of the set-up. A multizone (3…4 coils) resistance furnace 1 was fixed on a movable platform 2 that was moved along the rails 3 with a dc motor 4 via a special driving gear. This gear involved a reducer 5 and screw gear (worm gear) 6. A screw gear lead, reduction coefficient and motor rotation rate were chosen in such a way to ensure the possibility for velocity variation of furnace horizontal motion between 0.5 and 10 mm/h. Application of dc motor made it possible to vary smoothly the velocity of furnace motion over a preset range.

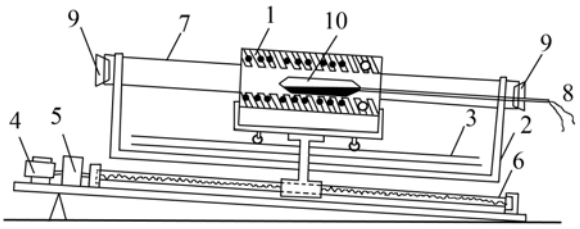

Fig. 1. Scheme of the set-up for production of SS crystals using horizontally-oriented crystallization.

An ampoule 10 of a particular shape with weights of the starting elements was moved in a quartz tube 7 that was fixed on the same axis as the furnace. The reactor temperature was monitored with chromel-alumel thermocouples 8 that were introduced through fireclay dummy plugs 9. Automatic recording of thermocouple readings was made using PC. The temperature of the resistance furnace coils was adjusted and kept with special electronic devices and autotransformers. To obtain big temperature gradients (50 to 70 °C/cm) in the crystallization zone, the latter (right) coil of the furnace was made as a spiral (coil diameter of 5…6 mm) of nichrome wire (diameter 1…1.2 mm). The set-up made it possible to keep temperature in the furnace within 1.5 °C.

When synthesizing SS, the temperature in the furnace first was increased (with the rate 70…80 °C/h) up to 550…600 °C, and then was kept at this level during 6 to 7 h, to ensure the diffusion of volatile components (Cd and Sb*)* into the melt. Then the temperature in the synthesis zone was increased up to 850–900 °C, to ensure an intense interdiffusion of the components and required degree of SS crystal homogeneity. The time of synthesis depended on the content of CdTe in SS; it was 10 (48) h at 0.1 (5) mol. % of CdTe in InSb.

The temperature distribution in the furnace when SS crystal growing using the horizontally-oriented crystallization technique is shown in Fig. 2. The temperature in the crystallization zone was 3 to 5 °C over that of crystallization. Then the mechanism of resistance furnace motion was started and the crystallization process proper began. Using this technique, we obtained SS crystals (mass up to 100 g, length up to 11 cm) with CdTe content up to 5 mol. %.

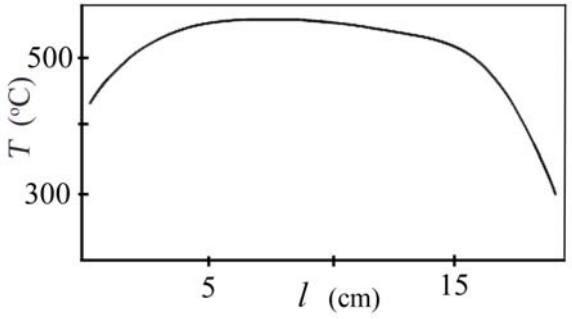

Fig. 2. Temperature distribution in the furnace.

When applying the above technique, one should give particular attention to choice of the magnitudes of the temperature gradient and velocity of furnace motion relatively to the stationary reactor. It is precisely these parameters that affect strongly the form of crystallization front. At a tiny temperature gradient and high velocity of crystallization front motion, the front becomes bent in the melt [4]. In this case, the cooling through the side surface occurs. This leads to spontaneous production of a great number of crystalline nuclei is a result of the polycrystalline growth. The optimal conditions for obtaining single or polycrystal samples were determined experimentally and were as follows: the temperature gradient of 50…70 °C/cm and velocity of crystallization front motion υ = 0.1…5 mm/h (it depends strongly on x – the content of CdTe in SS: the bigger is x, the lower should be υ).

The above crystallization conditions ensure uniformity in the cross-sections of the grown crystals. However, some variations of composition along the sample length still remain. So it is necessary to monitor the chemical composition and degrees of homogeneity and uniformity of the ingots. Such monitoring was realized using the X-ray spectrum analysis, X-ray diffraction analysis and fine-structural investigations (see [1]). The results obtained evidence that chemical composition of the middle part of the ingots is close to that of the starting weight of elements. The impurity distribution is practically uniform in the ingot middle part with a length of about 70 % of the total ingot length.

Our investigations of the Hall concentration and mobility of electrons showed that they vary non-monotonically with chemical composition of SS at 2–3 mol. % of CdTe (Table). In the middle part of the ingots (2/3 length), the departure of the concentration from the mean value did not exceed 15%, and the crystals were sufficiently uniform as concerned the Hall concentration of free charge carriers (electrons).

Fig. 3 demonstrates how the screw dislocation density in SS depends on the crystal composition and growth conditions. It was shown that, under the optimal crystallization conditions, the density D of screw dislocations in a purposely undoped InSb material was (3…6)×10^4 cm^{-2}; however, after addition of CdTe, it grew abruptly up to ~5×10^6 cm^{-2} at the impurity concentration of 1.5 to 2.5 mol. %. This evidences that the growth of SS crystal proceeds according to the layer-by-layer and dislocation mechanisms.

When studying the SS optical properties at room temperature, we used those crystals whose parameters are summarized in Table. They were flat plates, with the diameter from 10 up to 15 mm and thickness of 2 to 3 mm; their surface finish class was no less than 14. The experimental reflection spectra of SS (taken in the 200 to 4000 cm^{-1} frequency range) were registered using a spectrophotometer SPECORD-M80 with a reference mirror (for experimental procedure see [5]). The reflection coefficient values were determined within 1…2 %. The resolving ability in the above frequency range was 1 cm^{-1}.

Table. The concentration and Hall mobility of electrons in the $(InSb)_{1-x}(CdTe)_x$ crystals at the temperature 300 K.

# of the batch samples	CdTe content in SS (mol. %)	Electron concentrat. (cm^{-3})	Electron mobility (cm^{2}V^{-1}s^{-1})
1	0	(7.2±4.6)×10^{16}	(2.3±1.1)×10^4
2	0.0025	(3.5±1.2)×10^{18}	(6.2±3.8)×10^3
3	0.005	(8.4±7.3)×10^{18}	(8.2±7.1)×10^3
4	0.0075	(6.4±1.9)×10 ^{18}	(3.2±2.4)×10^3
5	0.01	(2.8±0.8)×10^{18}	(3.5±1.8)×10^3
6	0.02	(7.2±1.6)×10^{17}	(6.6±5.4)×10^3
7	0.03	(6.6±2.1)×10^{17}	(6.4±5.2)×10^3
8	0.04	(7.7 ±3.5)×10^{17}	(6.0±4.3)×10^3
9	0.05	(1.1±0.7)×10^{19}	(8.7±6.3)×10^2

3. Results of investigations of the optical and electrical properties of SS $(InSb)_{1-x}(CdTe)_x$ and discussion

The results of investigations of electrical and magnetic properties obtained in [1, 3, 6] indicate a complex character of interaction of Cd and Te impurity atoms between themselves, as well as with the InSb lattice. This leads to a nonmonotonous dependence of the lattice parameter and both concentration and mobility of charge carriers on SS chemical composition, as well as to appearance of peaks in the temperature dependence of the Hall constant, *etc*. There exist rather detailed discussions of investigations of optical and electrical properties of semiconductors performed using the nondestructive techniques of IR reflection and transmission spectroscopies [5, 7]. However, as to SS $(InSb)_{1-x}(CdTe)_x$ crystals, these problems practically were not considered.

Fig. 4 shows the experimental reflection coefficient as a function of the energy of incident photons for all the SS compositions. All the curves (numbers of which correspond to those in Table) have clearly pronounced typical minima that correspond to resonance absorption by free charge carriers. One can see that, as the photon energy increases, the $R(\nu)$ curve approaches 0.36 (for all the SS compositions), thus deriving for high-frequency permittivity the value ε_∞ = 16.

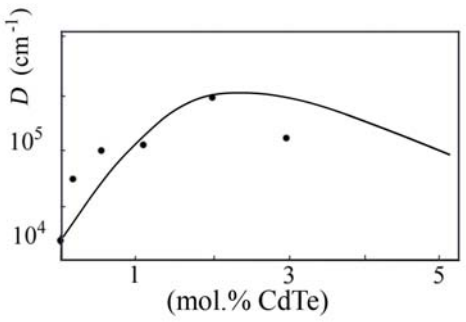

Fig. 3. Density of screw dislocations as a function of the CdTe content in SS.

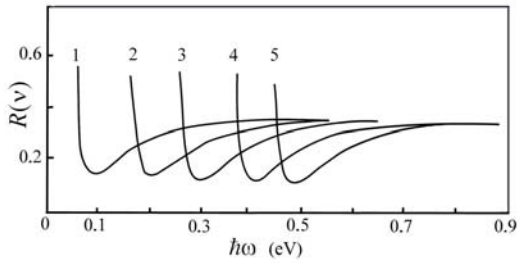

Fig. 4. The reflection coefficient of $(InSb)_{1-x}(CdTe)_x$ as a function of the energy of incident photons at various values of the CdTe content in SS *x*: *1* – 0.005; *2* – 0.0075; *3* – 0.01; *4* – 0.02; *5* – 0.03.

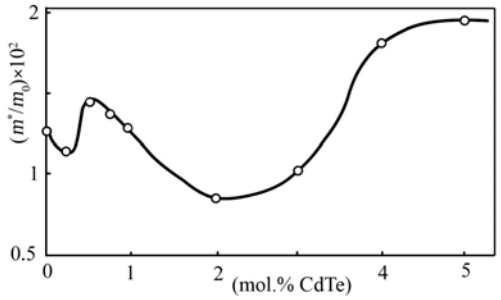

Fig. 5. The effective mass of charge carriers at the Fermi level as a function of the CdTe content in SS.

According to [1, 7], one can use the dependence of the position and depth of reflection coefficient minimum in heavily doped samples on the concentration, mobility and effective mass of charge carriers for determination of any of the above three quantities, if the other two are known. The concentration and mobility of free charge carriers (electrons) were determined from the Hall effect. The charge carrier effective mass m^* at the Fermi level was determined from the position of the reflection coefficient minimum. In our case, the error of m^* and ε_∞ determination did not exceed 10…15 %. The obtained dependence of the effective mass m^* at the Fermi level on the SS chemical composition is shown in Fig. 5.

By applying the Kane dispersion law, one can present the relationship between m^* and electron concentration n_0 as [8]:

$$\left(\frac{m^*/m_0}{1-m^*/m_0}\right)^2 = f\left(n_0^{2/3}\right), \qquad (1)$$

where m_0 is the free electron mass. Shown in Fig. 6a are the experimental $f\left(n_0^{2/3}\right)$ curves for various values of CdTe content *x*, while Fig. 6b shows the dependence of the InSb bandgap on the SS composition. For given *x*, the m^* values were determined from the concentration dependences of the reflection coefficient spectra. One can see from Fig. 6a that the experimental points fall on a straight line. This fact evidences that the Kane theory is applicable to all the SS compositions studied.

We determined the optical bandgap value E_g^{opt} for every SS composition from the lengths cut off by the straight lines on the ordinate axis (Fig. 6a). The dependences of the effective mass and optical bandgap on SS composition are complex and nonmonotonous (Fig. 6b). The minimal values, $m^*/m_0 = 0.8\cdot10^{-2}$ and $E_g^{\text{opt}} = 0.07$ eV, are observed for $x = 0.02…0.03$.

We concluded from the studies performed that the character of dependences of SS bandgap and effective mass on the SS composition (*x*) is determined unambiguously by the change of the crystal lattice parameter *a*(*x*). As *a*(*x*) increases (decreases), then $m^*/m_0(x)$ and E_g^{opt} decrease (increase). It was shown in [1] that the *a*(*x*) dependence is determined by complex character of interaction of dopant atoms between themselves, as well as with the InSb lattice. For SS $(InSb)_{1-x}(CdTe)_x$ the bandgap is much narrower than in pure indium antimonide. This fact makes SS more promising for fabrication of IR photodetectors.

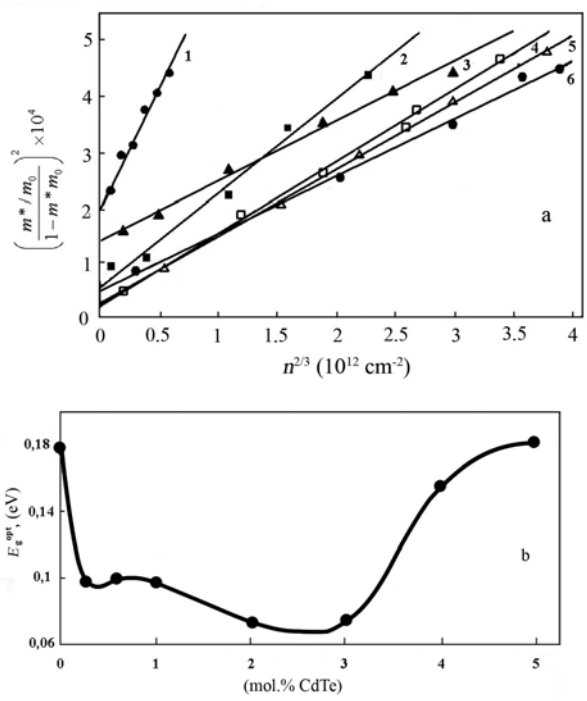

Fig. 6. a) $\left(\frac{m^*/m_0}{1-m^*/m_0}\right)^2 = f\left(n_0^{2/3}\right)$ at the various values of the CdTe content in SS *x*: *1* – 0.0025; *2* – 0.005; *3* – 0.0075; *4* – 0.01; *5* – 0.02; *6* – 0.03; b) InSb bandgap as a function of CdTe content in SS.

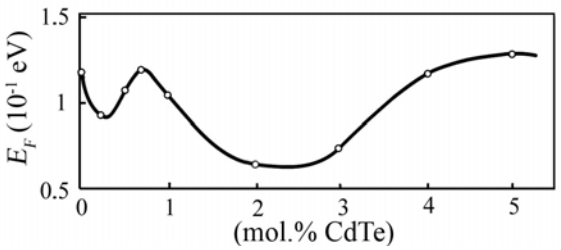

Fig. 7. The Fermi level (relative to the bottom of the conduction band) as a function of CdTe content in SS.

The m^* value can be estimated using the following expression [1]:

$$\frac{1}{m^*} = \frac{1}{m_0}\left(1 + \frac{E_g}{E_p}\right), \qquad (2)$$

where E_g is the direct gap between the edges of allowed bands, wave functions of which are of different symmetries (for example, *s*- and *p*-symmetry). It was found experimentally that $E_p \approx 20$ eV for all crystals with diamond- and sphalerite-type lattices [8]. The obtained m^* values are given in Fig. 5. One can see that the $m^* = f(x)$ curve follows, on the whole, that of $m_0(x)$.

According to [9], the dependence of the effective mass on the energy may be presented as

$$m^*(E) = m^*\left(1 + 2E / E_g^{\text{opt}}\right). \qquad (3)$$

Knowing the effective mass value at the Fermi level, one can estimate from Eq. (3) the energy $E = E_F$ corresponding to it. Using the $m^*(x)$ curves (Fig. 5) and E_g^{opt} value, one can determine the dependence of the Fermi level position (relatively to the conduction band edge) in the SS composition (Fig. 7).

Shown in Fig. 8 are the absorption coefficient *vs* photon energy curves, $k(\hbar\omega)$, for four crystals with various contents of Cd and Te. There are two growing portions of absorption curves (at high and low energies) that characterize interband transitions and absorption by free charge carriers, respectively. Using (at $\hbar\omega < 0.3$ eV) the known relation $k = A\lambda^p$ between *k* and wavelength λ of incident light (the power *p* depends on the charge carrier scattering mechanism), one can obtain information on the predominant scattering mechanism for each alloy.

It follows from Fig. 9 (where the $k(\lambda)$ curves are plotted on a log-log scale) that $p = 2$, 1.94 and 3.5 for $x =$ 0.0025, 0.05 and 0.03, respectively. The *p* values that are close to 2 are the characteristics of strongly degenerated materials. For these SS, earlier it was shown that the electron mobility does not depend on temperature over the wide temperature range (100 to 700 K). The values $p =$ = 3…3.5 are observed, if charge carriers are scattered by impurity ions. This conclusion was also reached from the analysis of the temperature dependence of the charge carrier mobility in 100…400 K temperature range: $\mu \approx T^{\alpha}$, with α close to 1.5. Thus, the conclusions concerning the mechanisms of electron scattering in alloys of various compositions (that were obtained from an analysis of the temperature dependences of charge carrier mobility) find their confirmation in the investigation of $k(\lambda)$ dependence in the region of free charge carrier absorption.

At higher energies, an analysis of the shape of low-energy edge of intrinsic absorption is complicated for several reasons. The most essential of them are as follows. When the charge carriers are strongly degenerated, then absorption of light by free charge carriers is superimposed on that near the low-energy edge; besides, the impurity states take part in optical transitions. The absorption by free charge carriers can be approximated from its shape in the low-energy region and then subtracted from the total absorption. After this is made, one can see that all the

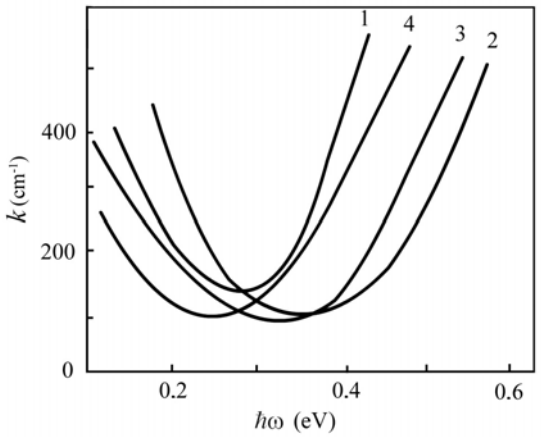

Fig. 8. Absorption coefficient spectral curves $k(\hbar\omega)$ for various values of the CdTe content in SS *x*: *1* – 0.0025; *2* – 0.05; *3* – 0.01; *4* – 0.03.

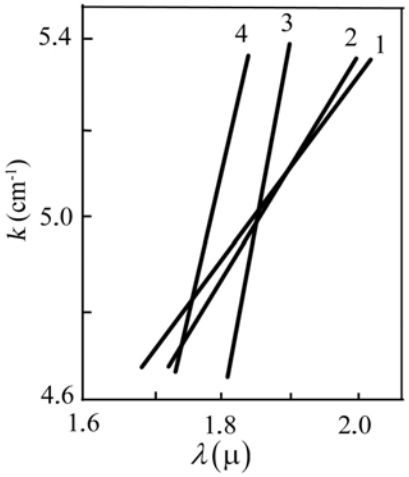

Fig. 9. Log-log scale dependence of free charge carrier absorption coefficient *k* on the light wavelength λ for various values of CdTe content in SS *x*: *1* – 0.0025; *2* – 0.05; *3* – 0.01; *4* – 0.03.

studied SS samples demonstrate exponential dependence of the optical absorption edge on photon energy (Fig. 10) (when this energy is below the bandgap). The characteristic energy E in the expression $k = k_0 \exp(\hbar\omega / E)$ for the absorption coefficient is the same (about 27 meV) for all SS, *i.e.*, it corresponds to the energy value kT for 300 K.

It is known [10] that the criterion for heavy doping can be applied to semiconductors, when the mean distance between the impurity atoms is much less than the Bohr radius of electron on a donor: $Na^3 >> 1$. Due to fluctuations of the concentration of charged impurities, the density of electron states in such materials does not vanish at the boundaries of allowed bands. It decreases in accordance with the exponential law when going deeper into the forbidden band [10]. The investigations of galvanomagnetic properties of a number of narrow-gap semiconductors, in particular, strongly compensated, showed that there is a deep potential relief of the conduction band bottom due to impurity aggregations. The depth of the most probable potential wells, γ, is 40 to 50 meV. Such wells have bound electron states. In this case, $\gamma\left(\hbar^2 / 2m_0 r_s^2\right)^{-1} \approx 2$, and electron tunneling through the barrier seems unlikely. So, such potential barrier may not lead to optical reduction of bandgap.

At the same time, we observed absorption of photons with energy deficiency: $\Delta = E_g^{\text{opt}} - \hbar\omega > 0$. In [11], it was shown that this is related to the presence of smaller-scale fluctuations of the charged impurity concentration. They result in shallow deformations of potential barriers against the background of deep potential wells. Due to a big difference between the effective mass values for electrons and holes in InSb, the electrons will not feel a shallower potential relief, while the holes (having a bigger effective mass) can have bound states in the shallow potential wells. In that case, spatial distribution of the valence band energy levels follows the small-scale potential relief, while the conduction band structure remains unchanged. As a result, the tail of density of states (that is responsible for absorption of photons whose energy is below the bandgap) appears at the valence (and not conduction) band. So, the absorption curve at $\hbar\omega < E_g^{\text{opt}}$ may be determined by electron transitions from the valence band tail to the conduction band bottom (distorted with the presence of impurities).

Now let us consider the curves of edge absorption in SS samples when $\hbar\omega < E_g^{\text{opt}}$. In this case, because the electron gas is strongly degenerated, the optical transitions from the valence band tail are to the levels lying deeply in the conduction band (near the Fermi level). At the temperature 300 K, the characteristic energy that enters into the exponential law for absorption edge is determined by the Fermi distribution of empty levels in the conduction band and is about 27 meV, *i.e.*, the kT value at 300 K.

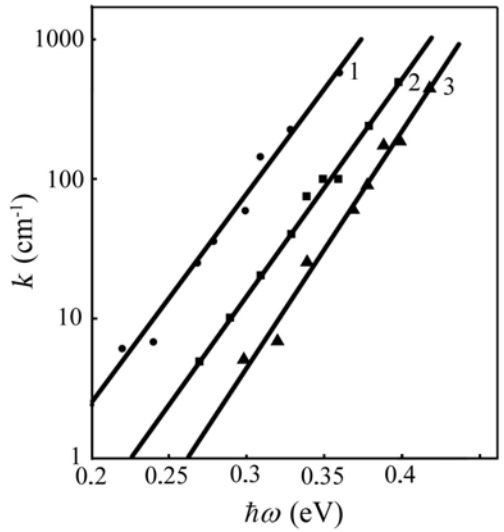

Fig. 10. Semilog scale spectral dependence of the absorption coefficient k for various values of CdTe content in SS x: *1* – 0.0025; *2* – 0.05; *4* – 0.03.

4. Conclusions

Our technological, physical-and-chemical and physical investigations demonstrated that the most promising manufacturing technique for perfect $(InSb)_{1-x}(CdTe)_x$ crystals ($x < 0.05$) is horizontal-oriented crystallization of melt with controlled pressure of volatile components. It was found that synthesis and melt crystallization should be combined in a single technological process. This makes it possible to decrease both the departure of SS chemical composition from the stoichiometric one and contamination with uncontrolled impurities. The required degrees of sample homogeneity and uniformity are obtained at high (800…830 °C) temperatures and long-term (up to 100 h) synthesis. Single-crystalline growth is ensured only by application of low (0.5…3.0 mm/h) velocities of crystallization front motion and rather high (50…70 K/cm) values of the crystallization temperature gradient.

A correlation was found between the dependences of the crystal lattice parameter, effective masses of charge carriers and optical bandgap on the chemical composition of SS crystals. A complicated character of these dependences is due to the features of interaction of the introduced impurity atoms between themselves and with the InSb lattice.

The principal parameters of SS band structure (optical bandgap and charge carrier effective mass at both the Fermi level and conduction band bottom) were determined for the samples with different contents of Cd and Te. It was shown that E_g^{opt} = 0.07 eV, when the composition x = 0.02, so the corresponding alloys are promising for fabrication of IR detectors.

An analysis of the intrinsic absorption edge in SS samples was performed. It was shown that, at small values of the absorption coefficient k, the light absorption is due to transitions between the tails of density of valence band states and the conduction band bottom. An assumption as to the possibility of formation in SS of neutral complexes that involve impurity atoms and those of the host lattice was confirmed. The free electron scattering mechanisms in SS of different compositions were determined.

References

1. V.A. Brodovoi, N.G. Vyalyi, and L.M. Knorozok // *Fizika Tekhnika Poluprov.* **32**, p. 303 (1998) [English translation: *Semiconductors* **32**, p. 274 (1998)].
2. V.A. Anischenko, V.A. Brodovoi, N.G. Vyalyi, V.A. Vikulov, and L.M. Knorozok // *Neorgan. Mater.* **29**, p. 197 (1993) (in Russian).
3. V.A. Brodovoi, V.G. Kolesnichenko, V.V. Skorokhod, A.V. Brodovoi, L.M. Knorozok, and O.S. Zinets // *Proc. SPIE* **4355**, p. 211 (2001).
4. A.Ya. Nashel'ski, *Production of semiconductor materials*. Metallurgiya, Moscow, 1989 (in Russian).
5. E.F. Venger, O.V. Melnichuk, and Yu.A. Pasichnyk, *Spectroscopy of residual rays.* Naukova Dumka, Kyiv, 2001 (in Ukrainian).
6. V.A. Brodovoi, A.V. Brodovoi, L.M. Knorozok, V.G. Kolesnichenko, and S.P. Kolesnik // *Fizika Tekhnika Poluprov.* **31**, p. 1052 (1997) [English translation: *Semiconductors* **31**, p. 899 (1997)].
7. J.I. Pancove, *Optical processes in semiconductors.* Dover Publications, New York, 1976.
8. I.M. Tsidilkovski, *Electron spectrum of gapless semiconductors*. Springer Verlag, 1997.
9. R. Dornhaus, G. Nimtz, and B. Schlicht, *Narrow gap semiconductors.* Springer, Berlin, 1983.
10. E.M. Omel'yanovskii, V.I. Fistul', L.A. Balagurov, V.S. Ivleva, V.V. Karataev, M.G. Mil'vidskii, A.N. Popkov // *Fizika Tekhnika Poluprov.* **9**, p. 576 (1975) (in Russian).
11. B.I. Shklovskii and A.L. Efros, *Electronic properties of doped semiconductors*. Springer, Berlin, 1984.